ChemComm

COMMUNICATION

View Article Online
View Journal | View Issue

Cite this: *Chem. Commun.*, 2023, **59**, 12120

Received 7th July 2023,
Accepted 8th September 2023

DOI: 10.1039/d3cc03277a

rsc.li/chemcomm

Time-, space- and energy-resolved *in situ* characterization of catalysts by X-ray absorption spectroscopy†

Stefan Peters,[a] Benny Kunkel,[a] Cafer Tufan Cakir,[b] Anke Kabelitz,[b] Steffen Witte,[b] Thomas Bernstein,[b] Stephan Bartling,[a] Martin Radtke,[b] Franziska Emmerling,[b] Ali Mohamed Abdel-Mageed,[a] Sebastian Wohlrab *[a] and Ana Guilherme Buzanich *[b]

A setup for dispersive X-ray absorption spectroscopy (XAS) with spatial, temporal and energy resolution is presented. Through investigation of a Mo/HZSM-5 catalyst during the dehydroaromatization of methane we observed a reduction gradient along the packed bed. Our new method represents an unprecedented addition to the analytical toolbox for *in situ* characterizations.

The characterization of catalysts under reaction conditions (*in situ*) or with simultaneous activity measurements during their operation (*operando*[1]) is a cornerstone for the in-depth understanding of catalytic processes and materials.[2] Compared to analysis *ex situ*, these methods allow investigating dynamic processes, transient products and active sites.[3] Raman,[4,5] infrared,[6] nuclear magnetic resonance,[7] electron paramagnetic resonance[8] or X-ray spectroscopies[9–11] have been successfully demonstrated and are invaluable for improved catalyst and process designs. However, demanding parameters such as high operating temperatures and pressures impose difficulty on *operando* characterization. Nevertheless, the insights possible with such methods can be highly important, especially in the field of heterogeneous catalysis. Fundamental knowledge in catalytic materials at work, such as electronic structure and local coordination environment, is essential to acquire information about the nature of the active sites and to establish a link between structural motifs and activity in a catalyst. One of the most common techniques is X-ray absorption spectroscopy (XAS).[12] A recent review of the challenges and opportunities for X-ray spectroscopy in catalysis research is given by Cutsail III and DeBeer.[13] For time resolved studies the two most prominent modes are quick XAS[14] and dispersive XAS.[15,16] With dispersive XAS the advantage for characterizing catalysts at work is that the whole energy range interacts with the sample and, with our setup, a large beam of a few mm^2 allows the extraction of time-, space- and energy-resolved information in a scanningless mode.[17,18]

One particular catalytic conversion where *in situ* analysis is of special interest is methane dehydroaromatization (MDA).[19] This reaction allows the production of ethylene, light aromatics and hydrogen at high temperatures ($\geq$600 °C) in the absence of oxidants.[20] The most researched and widely used type of catalyst for this reaction is molybdenum on various types of acidic zeolites, most prominently HZSM-5.[21–23] The MoO_3 on the catalyst is converted to oxycarbidic or carbidic species during the onset of the reaction before aromatics are produced (see Fig. 1A).[24–26] The utilization of *in situ* and *operando* characterization methods,[27–29] isotopic labeling[30,31] as well as DFT calculations[32,33] have been crucial for the elucidation of structure–activity relationships, but there is still no clear consensus about the exact reaction mechanism or structures of active sites. Furthermore, catalysts suffer from constant deactivation due to coking, particle agglomeration and dynamic transformation of Mo species.[34,35] The generation and stability of active Mo species is key for MDA catalysts. A common method to investigate the electronic properties of this element is X-ray photoelectron spectroscopy (XPS), which is surface sensitive,[36] thus not allowing bulk observation of species in the zeolite pores. In addition, the combination of the method with the catalytic experiment must be carried out at very low pressures to ensure sufficient photoelectron flux, which in turn weakens the validity of currently reported *in situ* XPS results.[9] However, XAS can be more easily performed under realistic reaction conditions. In contrast to homogeneous catalysis or reactions in stirred tanks, the concentrations of reactants and products change significantly along a heterogeneous catalyst bed as the reaction progresses. This is the case in many industrial catalytic reactions, as they are conducted under continuous reactant/product flow through packed beds. Considering the

[a] *Leibniz Institute for Catalysis (LIKAT Rostock), Albert-Einstein-Str. 29a, Rostock 18059, Germany. E-mail: sebastian.wohlrab@catalysis.de*
[b] *Federal Institute for Materials Research and Testing (BAM), Richard-Willstätter-Str. 11, Berlin 12489, Germany. E-mail: ana.buzanich@bam.de*

† Electronic supplementary information (ESI) available: Additional experimental details, XPS tables, catalysis and TPR results. See DOI: https://doi.org/10.1039/d3cc03277a

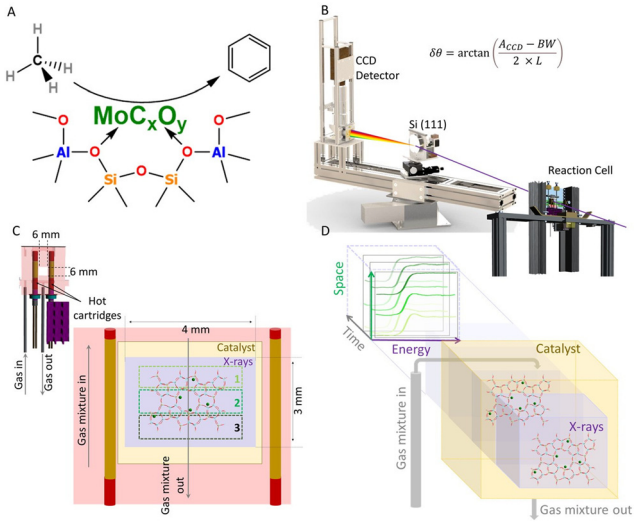

Fig. 1 (A) Simplified scheme of the MDA reaction on Mo/HZSM-5 catalysts; (B) Sketch of the experimental *in situ* XAS setup; (C) Cross-section view of the measurement cell including a zoom-in showing the different sample regions and exemplary catalyst structure; (D) Visualization of the concept for time, space, and energy resolution.

gradually different fluid-phase compositions along the packed catalyst, it can also consequently impose a change upon the active material. Thus, it must be noted that knowledge of the true nature of a heterogeneous catalyst at work is often poorly understood. For our specific catalytic case Lezcano-González *et al.*[28] and Kosinov *et al.*[30] used *operando* XAS to investigate the dynamic change of Mo in methane at 700 °C. However, to our knowledge, the possible influence of concentration gradients of reactants and products was not yet considered in these characterizations. Nevertheless, research has shown that pretreatment of Mo/HZSM-5 in different gas compositions can lead to different catalytical properties, suggesting the formation of active sites with slightly altered physicochemical attributes.[4,37,38] With respect to MoO_3, the different reactivities of CH_4 compared to the products H_2,[39] C_2H_4[40] and C_2H_6[41] could have an impact on the structure and formation rate of active sites. In this context Song *et al.*[42,43] reported significant disparities in coke deposition on spent Mo/HZSM-5 in different catalyst layer positions at 800 °C. The inlet layer exhibited increased polyaromatic coke compared to the outlet layer, presumably due to product concentration and selectivity gradients along the catalyst bed. Unfortunately, literature results from *in situ* or *operando* catalyst characterizations by XAS are obtained by averaging over the reactor space.[30]

The focus of this work is the demonstration of spatial resolution in an *in situ* investigation in addition to observations over time on stream for a deeper insight into the transformation mechanisms of catalytically active species. As an exemplary system we chose a Mo/HZSM-5 catalyst for MDA (see Fig. 1A). We introduce a new, custom-designed dispersive XAS setup to explore possible space-dependent differences in Mo speciation. This innovative approach allows both space- and time-resolved energy spectra to be measured *in situ*. The experimental setup is depicted in Fig. 1B (further technical information in the ESI†).

XAS measurements were performed at the synchrotron BESSY II in Berlin, Germany. The setup for time-, space- and energy-resolved XAS was installed at the BAM*line*.[18] The incident polychromatic X-ray beam is generated by a Pd mirror together with a 60 μm thick Al filter (spectral flux visualized in Fig. S1, ESI†). A schematic view of the measurement cell and structure of the Mo/HZSM-5 is shown in Fig. 1C. The sample cell is made of Inconel steel and is equipped with a SiN window, gas connections and two heating cartridges controlled by a thermocouple. The sample cavity has an area of approximately 6 × 6 mm^2. The X-ray beam used was 4 mm wide and 3 mm high, resulting in a total illuminated area of 4 × 3 mm^2. Control experiments have shown temperature differences below 10 K up to 800 °C. The transmitted beam is diffracted by a convex Si(111) crystal and recorded by a CCD detector (see also Fig. S1, ESI†). This setup allows the detection of the entire XAS spectrum in one shot for the whole illuminated area (Fig. 1D). Spatial resolution is achieved by dividing the area into three regions: 1 being the top, 2 the middle, and 3 the bottom (see Fig. 1C). This promotes our setup to a novel and unique ability to characterize catalyst materials *in situ* with a 3-dimensional reference.

We first investigated our Mo/HZSM-5 catalyst by XPS before and after treatment in methane at 600 °C (see Fig. 2, also Table S2, ESI†) for comparison with our new method. The obtained results show a partial reduction of molybdenum along with a deposition of carbon. Contributions of Mo^{6+} (232.9 eV), Mo^{5+} (231.8 eV), Mo^{4+} (230.5 eV, 229.3 eV) and Mo^{2+} (228.9 eV, 228.3 eV) were assigned and deconvoluted using literature ref. 9 with binding energies given for the respective Mo $3d_{5/2}$ signals (± 0.1 eV). Mo^{5+} can in this case be regarded as stabilized species on Brønsted acid sites.[44] Metallic Mo^0 was not detected. To further elucidate the formation of these different molybdenum states *operando* near-ambient pressure XPS (NAP-XPS) was performed (see Table S3, ESI†). By increasing

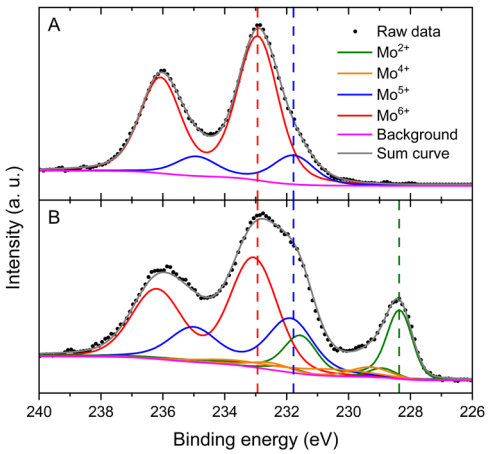

Fig. 2 XPS spectra at the Mo 3d level recorded *ex situ* of fresh 6Mo/HZSM-5 (A) and spent sample after 360 min of reaction with 90% CH_4/10% N_2 at 600 °C (B), showing partial transformation of Mo to (oxy-)carbidic species. Dashed lines corresponding to the Mo $3d_{5/2}$ binding energies of Mo^{6+}, Mo^{5+} and Mo^{2+} are added as a visual aid.

the temperature of the sample in a CH_4 atmosphere at 2 mbar a stepwise reduction of Mo^{6+} to Mo^{4+} was observed, while Mo^{2+} formation occurred only after a prolonged reaction time. Lezcano-Gonzáles *et al.*[28] also concluded from their *operando* XAS studies that Mo is carburized stepwise. Methane pulsing resulted in similarly staggered changes as the reduced reaction pressure of our NAP-XPS measurements. However, the required pressure gap and surface sensitivity limit the power of NAP-XPS for *in situ* characterization of MDA catalysts.

Both our *ex situ* and *operando* XPS investigations proved the coexistence of oxidic and carbidic Mo species. As methane and MDA products show different reduction/carburization potentials, these compounds might form inhomogeneously over the catalyst bed.[45–47] In order to follow a possible reduction gradient within the catalyst at work, we performed unprecedented spatially resolved XAS measurements at ambient pressure. Fig. 3 shows the recorded X-ray absorption data. The rows labeled with regions 1, 2 and 3 refer to the spatial resolution depicted in Fig. 1C. The columns are divided into selected XANES curves at different temperatures (Fig. 3A, D and G), their respective derivatives (Fig. 3B, E and H) and projections of the derivative curves over the whole measurement (Fig. 3C, F and I). From the XANES curves in all regions an absorption maximum at approximately 20 020 eV is clearly visible from the beginning of the experiment until 520 °C (1500 s). This energy is comparable to the MoO_3 reference (blue curve in Fig. S2A, ESI†) and

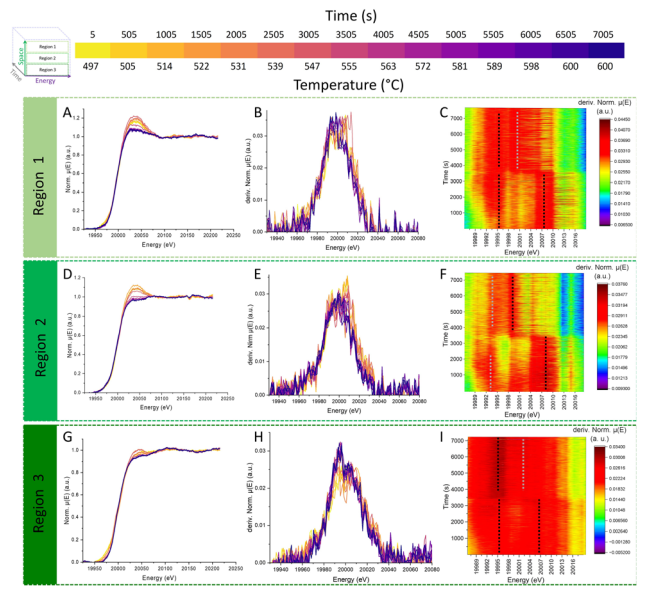

Fig. 3 Three-dimensionally resolved *in situ* XAS investigations of 6Mo/HZSM-5 during ambient pressure MDA in 20% CH_4/80% N_2. Measurements were divided into different segments (from inlet to outlet regions 1, 2, 3). For each region, the XANES curves (left column, A, D, G), the corresponding derivatives (middle column, B, E, H), sum of every 60 seconds, and the projection of the derivative curves over the whole experiment with a time resolution of 5 s (right column, C, F, I) are shown. The colors of the lines in the first two columns correspond to the time/temperature plotted at the top of the figure. In the third column, dashed lines corresponding to strong (black) and weak (grey) maxima are added as a visual aid.

signifies the dominant initial state of Mo as proven by XPS (see Fig. 2). From 555 °C this absorption maximum decreases in region 1, while in regions 2 and 3 it vanishes completely. This indicates the loss of MoO_3 species through reduction by CH_4. Both the derivative curves and heat maps clearly show two maxima (19 994 ± 1 eV and 20 007 ± 1 eV, see Fig. 3B, E and H) until 520 °C, which again fit well with the first derivative plot of MoO_3 (see Fig. S2B, ESI†). The former maximum reveals a pre-peak transition (1s → 4d) which is more likely to occur in tetrahedrally coordinated environments.[48] From 555 °C the second maximum at 20 007 ± 1 eV disappears, indicating a partial reduction of MoO_3. a new maximum is observed at 20 001 ± 1 eV, while 19 994 ± 1 eV becomes the strongest maximum in region 3. Both fit well to the maxima observed for the MoC and Mo_2C references (red and purple curves in Fig. S2B, ESI†). Furthermore, the XANES curves in region 3 reveal new features between 20 060–20 100 eV, which also indicate the formation of MoC or Mo_2C. From these observations it can be concluded that the reaction with methane at 600 °C produces a mixture of Mo oxide and carbide species. The reduction of Mo begins at 520 °C, resulting in a diminishment of the oxide contribution in the obtained spectra. The regional XANES and derivative curves indicate that the concentration of MoO_x species decreases over the length of the catalyst bed while the relative concentration of MoC_x species increases inversely. The observation of both oxidic and carbidic species agrees with our XPS results. The differences in Mo speciation in dependence of relative position in the reactor can be explained by the characteristics of the MDA reaction itself. Upon contact with CH_4 MoO_3 is reduced to create active sites. During this initial activation process, only CO_x, H_2 and possibly H_2O are formed. This is also visible from our MDA experiments in a conventional plug flow reactor, resulting in ~7% methane conversion, high CO_x selectivity and no aromatics formation at 30 min on stream at 600 °C (see Fig. S3, ESI†). As CH_4 is consumed while flowing through the catalyst bed, the amount of H_2 increases. This *in situ* formed hydrogen may facilitate downstream reduction of MoO_3. Literature studies of temperature-programmed reduction (TPR)[45] by H_2 and temperature-programmed surface reaction (TPSR)[46] by CH_4 reveal a significant difference in reduction potential. While Mo^{6+} is reduced to Mo^{4+} at temperatures >600 °C in methane, a first reaction occurs at temperatures 100–150 °C lower in diluted hydrogen.[47] Our own TPR experiments (see Fig. S4, ESI†) show similar reduction behaviour. Furthermore, it has been demonstrated that C_{2+} hydrocarbons can carburize Mo oxides at lower temperatures than CH_4.[49] The concentration gradient of CH_x fragments and C–C coupled products in packed bed reactors may thus be responsible for the more severe carburization of Mo species we observe near the outlet.

In summary, the addition of spatial resolution to XAS is an important step in improving the understanding of catalytic materials in operation. We have shown that the change in reactant and product concentrations along a catalyst bed should not be neglected and can lead to the formation of different species. The knowledge gained from this new type of characterization could improve rational catalyst design,

especially for industrial applications where reactors are large, and conversions are typically high.

This research was funded by the Deutsche Forschungsgemeinschaft (DFG), grant number 351914377. The authors would like to thank Dr Kirill Yusenko, Ralf Britzke, Michael Sintschuk, and Sven Schlau (BAM) for analytical and technical support. Experiments were performed at the BAM*line* at the BESSY-II storage ring (Helmholtz-Zentrum Berlin für Materialien und Energie, HZB).[18] We thank the HZB for the allocation of synchrotron radiation beamtime.

Conflicts of interest

There are no conflicts to declare.

Notes and references

1 B. M. Weckhuysen, *Chem. Commun.*, 2002, 97–110.
2 M. A. Bañares, *Catal. Today*, 2005, **100**, 71–77.
3 F. Zaera, *J. Catal.*, 2021, **404**, 900–910.
4 W. Li, G. D. Meitzner, R. W. Borry and E. Iglesia, *J. Catal.*, 2000, **191**, 373–383.
5 P. Waleska, S. Rupp and C. Hess, *J. Phys. Chem. C*, 2018, **122**, 3386–3400.
6 C. Lamberti, A. Zecchina, E. Groppo and S. Bordiga, *Chem. Soc. Rev.*, 2010, **39**, 4951–5001.
7 E. D. Walter, L. Qi, A. Chamas, H. S. Mehta, J. A. Sears, S. L. Scott and D. W. Hoyt, *J. Phys. Chem. C*, 2018, **122**, 8209–8215.
8 V. T. T. Ha, A. Sarioglan, A. Erdem-Senatalar and Y. Ben Taarit, *J. Mol. Catal. A: Chem.*, 2013, **378**, 279–284.
9 K. Murugappan, E. M. Anderson, D. Teschner, T. E. Jones, K. Skorupska and Y. Román-Leshkov, *Nat. Catal.*, 2018, **1**, 960–967.
10 M. Agote-Arán, A. B. Kroner, H. U. Islam, W. A. Sławiński, D. S. Wragg, I. Lezcano-González and A. M. Beale, *ChemCatChem*, 2019, **11**, 473–480.
11 Y. Liu, H. Zhang, A. S. G. Wijpkema, F. J. A. G. Coumans, L. Meng, E. A. Uslamin, A. Longo, E. J. M. Hensen and N. Kosinov, *Chem. – Eur. J.*, 2022, **28**, e202103894.
12 J. Timoshenko and B. Roldan Cuenya, *Chem. Rev.*, 2021, **121**, 882–961.
13 G. E. Cutsail III and S. DeBeer, *ACS Catal.*, 2022, **12**, 5864–5886.
14 M. Nachtegaal, O. Müller, C. König and R. Frahm, in *X-Ray Absorption and X-Ray Emission Spectroscopy*, ed. J. A. van Bokhoven and C. Lamberti, 2016, pp. 155–183.
15 J. Huang, B. Günther, K. Achterhold, Y.-T. Cui, B. Gleich, M. Dierolf and F. Pfeiffer, *Sci. Rep.*, 2020, **10**, 8772.
16 A. S. Leach, J. Hack, M. Amboage, S. Diaz-Moreno, H. Huang, P. L. Cullen, M. Wilding, E. Magliocca, T. S. Miller, C. A. Howard, D. J. L. Brett, P. R. Shearing, P. F. McMillan, A. E. Russell and R. Jervis, *J. Phys.: Condens. Matter*, 2021, **33**, 314002.
17 A. Kulow, S. Witte, S. Beyer, A. Guilherme Buzanich, M. Radtke, U. Reinholz, H. Riesemeier and C. Streli, *J. Anal. At. Spectrom.*, 2019, **34**, 239–246.
18 A. Guilherme Buzanich, M. Radtke, K. V. Yusenko, T. M. Stawski, A. Kulow, C. T. Cakir, B. Röder, C. Naese, R. Britzke, M. Sintschuk and F. Emmerling, *J. Chem. Phys.*, 2023, **158**, 244202.
19 I. Vollmer, I. Yarulina, F. Kapteijn and J. Gascon, *ChemCatChem*, 2019, **11**, 39–52.
20 J. J. Spivey and G. Hutchings, *Chem. Soc. Rev.*, 2014, **43**, 792–803.
21 N. A. Mamonov, E. V. Fadeeva, D. A. Grigoriev, M. N. Mikhailov, L. M. Kustov and S. A. Alkhimov, *Russ. Chem. Rev.*, 2013, **82**, 567–585.
22 N. Kosinov and E. J. M. Hensen, *Adv. Mater.*, 2020, **32**, 2002565.
23 N. Elrefaei, N. Basha, M. Nounou, H. Nounou, A. Ashok and M. Al-Rawashdeh, *ChemCatChem*, 2022, **14**, e202200711.
24 D. Wang, J. H. Lunsford and M. P. Rosynek, *Top. Catal.*, 1996, **3**, 289–297.
25 Y. Shu and M. Ichikawa, *Catal. Today*, 2001, **71**, 55–67.
26 H. Zheng, D. Ma, X. Bao, J. Z. Hu, J. H. Kwak, Y. Wang and C. H. F. Peden, *J. Am. Chem. Soc.*, 2008, **130**, 3722–3723.
27 J. Gao, Y. Zheng, J.-M. Jehng, Y. Tang, I. E. Wachs and S. G. Podkolzin, *Science*, 2015, **348**, 686–690.
28 I. Lezcano-González, R. Oord, M. Rovezzi, P. Glatzel, S. W. Botchway, B. M. Weckhuysen and A. M. Beale, *Angew. Chem., Int. Ed.*, 2016, **55**, 5215–5219.
29 M. Agote-Arán, R. E. Fletcher, M. Briceno, A. B. Kroner, I. V. Sazanovich, B. Slater, M. E. Rivas, A. W. J. Smith, P. Collier, I. Lezcano-González and A. M. Beale, *ChemCatChem*, 2020, **12**, 294–304.
30 N. Kosinov, A. S. G. Wijpkema, E. A. Uslamin, R. Rohling, F. J. A. G. Coumans, B. Mezari, A. Parastaev, A. S. Poryvaev, M. V. Fedin, E. A. Pidko and E. J. M. Hensen, *Angew. Chem., Int. Ed.*, 2018, **57**, 1016–1020.
31 I. Vollmer, B. van der Linden, S. Ould-Chikh, A. Aguilar-Tapia, I. Yarulina, E. Abou-Hamad, Y. G. Sneider, A. I. Olivos Suarez, J.-L. Hazemann, F. Kapteijn and J. Gascon, *Chem. Sci.*, 2018, **9**, 4801–4807.
32 T. S. Khan, S. Balyan, S. Mishra, K. K. Pant and M. A. Haider, *J. Phys. Chem. C*, 2018, **122**, 11754–11764.
33 G. Li, I. Vollmer, C. Liu, J. Gascon and E. A. Pidko, *ACS Catal.*, 2019, **9**, 8731–8737.
34 V. I. Zaikovskii, A. V. Vosmerikov, V. F. Anufrienko, L. L. Korobitsyna, E. G. Kodenev, G. V. Echevskii, N. T. Vasenin, S. P. Zhuravkov, E. V. Matus, Z. R. Ismagilov and V. N. Parmon, *Kinet. Catal.*, 2006, **47**, 389–394.
35 C. H. L. Tempelman and E. J. M. Hensen, *Appl. Catal., B*, 2015, **176–177**, 731–739.
36 F. A. Stevie and C. L. Donley, *J. Vac. Sci. Technol., A*, 2020, **38**, 063204.
37 P. Tan, *Catal. Commun.*, 2018, **103**, 101–104.
38 A. Sridhar, M. Rahman and S. J. Khatib, *ChemCatChem*, 2018, **10**, 2571–2583.
39 H. Jiang, L. Wang, W. Cui and Y. Xu, *Catal. Lett.*, 1999, **57**, 95–102.
40 I. Vollmer, E. Abou-Hamad, J. Gascon and F. Kapteijn, *ChemCatChem*, 2020, **12**, 544–549.
41 H. Saito and Y. Sekine, *RSC Adv.*, 2020, **10**, 21427–21453.
42 Y. Song, Y. Xu, Y. Suzuki, H. Nakagome and Z.-G. Zhang, *Appl. Catal. A*, 2014, **482**, 387–396.
43 Y. Song, Y. Xu, Y. Suzuki, H. Nakagome, X. Ma and Z.-G. Zhang, *J. Catal.*, 2015, **330**, 261–272.
44 Y. Song, C. Sun, W. Shen and L. Lin, *Appl. Catal., A*, 2007, **317**, 266–274.
45 A. Martinez and E. Peris, *Appl. Catal. A*, 2016, **515**, 32–44.
46 N. Kosinov, F. J. A. G. Coumans, E. A. Uslamin, A. S. G. Wijpkema, B. Mezari and E. J. M. Hensen, *ACS Catal.*, 2017, **7**, 520–529.
47 K. Sun, W. Gong, K. Gasem, H. Adidharma, M. Fan and R. Chen, *Ind. Eng. Chem. Res.*, 2017, **56**, 11398–11412.
48 A. Gaur, M. Stehle, K. V. Raun, J. Thrane, A. D. Jensen, J.-D. Grunwaldt and M. Høj, *Phys. Chem. Chem. Phys.*, 2020, **22**, 11713–11723.
49 T. Xiao, A. P. E. York, K. S. Coleman, J. B. Claridge, J. Sloan, J. Charnock and M. L. H. Green, *J. Mater. Chem.*, 2001, **11**, 3094–3098.